Materials Chemistry and Physics 241 (2020) 122275

Contents lists available at ScienceDirect

Materials Chemistry and Physics

journal homepage: www.elsevier.com/locate/matchemphys

Improvement of corrosion penetration resistance for aluminum heat exchanger by alloying zirconium

Yong-Sang Kim [a], In-Jun Park [a], Byeong-Seon An [a], Jong Gil Park [b], Cheol-Woong Yang [a], Young Hee Lee [b], Jung-Gu Kim [a,*]

[a] School of Advanced Materials Science and Engineering, Sungkyunkwan University, 2066, Seobu-Ro, Jangan-Gu, Suwon, Gyeonggi-Do, 16419, Republic of Korea
[b] Center for Integrated Nanostructure Physics, Institute for Basic Science, Department of Energy Science, Sungkyunkwan University, 2066, Seobu-Ro, Jangan-Gu, Suwon, Gyeonggi-Do, 16419, Republic of Korea

HIGHLIGHTS

- In salt-water acetic acid solution, penetration depth of Zr added Al alloy was significantly decreased.
- Refinement of Al13Fe4 precipitates was observed by addition of Zr.
- Addition of Zr on Al alloy changed tendency of localized corrosion to uniform corrosion.

ARTICLE INFO

Keywords:
Aluminium alloy
Refinement
Corrosion
Zirconium
Intermetallic
Heat exchanger

ABSTRACT

Corrosion of the aluminum multi-port extrusion (MPE) leads to heat exchanger leakage. Corrosion of the 1xxx series aluminum MPE tubes proceeds continuously along $Al_{13}Fe_4$, which is the precipitation phase of Fe impurity. The continuous corrosion behavior along $Al_{13}Fe_4$ rapidly propagates into the aluminum MPE tube, thereby reducing the penetration life. In this study, Zr was added in order to control the dispersion of $Al_{13}Fe_4$ precipitates in an attempt to improve the corrosion resistance of A1070 aluminum MPE tubes for heat exchangers. The refinement and dispersion of $Al_{13}Fe_4$ phase was controlled by the addition of Zr, which is a highly insoluble element in aluminum. Zr plays a role in increasing nucleation and inhibiting the growth of the surrounding $Al_{13}Fe_4$ phase during the precipitation to $A_{l3}Zr$ phase. As a result, the size of the $Al_{13}Fe_4$ phase became finer and more dispersed, and the continuous corrosion tendency was decreased. Therefore, corrosion propagation of aluminum MPE tube progressed uniformly and penetration was suppressed.

1. Introduction

For years, aluminum (Al) and aluminum alloys have been used as heat exchanger tube materials due to their low density, good thermal conductivity, and satisfactory mechanical properties that are suitable for heat exchangers [1–4]. Al heat exchangers are used in various applications, such as air-conditioners, refrigerators, heat pumps in automobiles, and the aircraft industry. Recently, multi-port extrusion (MPE) tubes that can reduce the weight and volume of Al heat exchangers have been introduced. MPE tubes have a larger transfer area and smaller refrigerant-side volume than plate- or round-type tubes. Previous studies have reported that the overall heat transfer efficiency of an MPE heat exchanger is 62% higher than that of a plate-type condenser, even with 23% less refrigerant content [5–8]. As the tube becomes thinner, the corrosion resistance has a larger effect. According to results that have been obtained in the actual field, the corrosion penetration shape where the MPE Al tube leaked has been reported as a localized form of corrosion including intergranular and pitting corrosion [6,7]; Min and Webb, 2002). Therefore, studies should be conducted to prevent the corrosion penetration of Al MPE tubes.

1.1. Corrosion behavior of Al MPE tube

There are two causes of local corrosion in Al MPE tubes. The first involves the passive film of Al oxide. Protective passive oxide films can suppress the corrosion of Al in neutral atmospheres while locally damaged passive films will lead to more rapid corrosion [9,10]. The second cause involves the presence of an element in Al. Most dissimilar metals of Al impurities or alloying elements will form intermetallic (IM)

* Corresponding author.
E-mail address: kimjg@skku.edu (J.-G. Kim).

https://doi.org/10.1016/j.matchemphys.2019.122275
Received 22 September 2018; Received in revised form 28 June 2019; Accepted 7 October 2019
Available online 11 October 2019

Nomenclature

MPE	Multi-port extrusion
IM	Intermetallic
Al	Aluminum
Fe	Iron
Cu	Copper
Zr	Zirconium
Si	Silicon
SWAAT	Salt-water acetic acid test
FE-SEM	Field emission scanning electron microscopy
EDS	Energy dispersion spectroscopy
FE-EPMA	Field emission electron probe micro analyzer
HR-TEM	High resolution transmitted electron microscopy
SADP	Selected area diffraction pattern

Table 1
Chemical compositions of A1070 and U1070 (wt%).

Materials	Fe	Cu	Si	Zr	Al
A1070	0.1104	0.0046	0.1519	–	Rem.
U1070	0.1087	0.0037	0.1498	0.1491	Rem.

compounds with Al. When these IM compounds have different electrochemical potentials than the Al matrix, the local currents on the alloy surface will differ, establishing anodes and cathodes known as the micro-galvanic reaction.

Two types of localized corrosion behavior are caused by IM particles in Al alloy [11]; Pearson, 2008). The first one involves circumferential pits that appear as a ring of attack around more noble IM particles compared to pure Al matrix, such as iron (Fe) and copper (Cu). The second morphology is a selective dissolution of constituent particles that are more active IM particles compared to the Al matrix, such as Mg and Zn. In other words, IM particles with different electrochemical potentials with Al will either accelerate the corrosion of the surrounding Al or preferentially corrode over the Al matrix. In a tropical coastal climate environment, when the Al heat exchanger is destroyed, the Al passive film will be damaged due to the high concentration chloride attack. The micro-galvanic corrosion between Al matrix and IM particles has a dominant effect on localized corrosion initiation and propagation, thus inducing leakage in the MPE Al heat exchanger tube.

Al 1xxx series Al alloys are the most commonly used MPE Al tubes. The impurities or alloying elements such as Cu and Fe present in Al 1xxx Al will lead to localized corrosion penetration by forming IM particles with higher potential than the Al matrix. In order to reduce the corrosion propagation of the Al tube, Cu and Fe must be controlled. Our previous study [9] reported the influence of copper concentration on localized corrosion propagation of the Al tube alloy. Copper, a typical alloying element or impurity of Al alloy, can precipitate into Al_2Cu phase along the grain boundary at a concentration exceeding the solubility limit. These Al_2Cu, at a size of a few tens of nanometers, can accelerate the corrosion rate of the surrounding Al base material, causing the corrosion of Al to propagate continuously following the grain boundary. A previous study suggested that, in order to reduce corrosion penetration, the copper impurity concentration should be below 0.01 wt%, which is a lower value than the solubility limit of copper in Al. Fe is also a critical impurity of Al corrosion. In the Al–Fe phase diagram, the solubility of Fe at room temperature is below 0.01 wt%. Therefore, it is precipitated as Al_3Fe [12]. Several studies have reported that $Al_{13}Fe_4$ also accelerates the corrosion rate and causes local corrosion in Al, similarly to Al_2Cu [13–16]. Unfortunately, for economic reasons, lowering the concentration of Fe impurity is more difficult than lowering that of copper impurity.

1.2. Strategy to inhibit corrosion penetration of aluminum MPE tube

This study aims to improve the corrosion penetration durability of Al 1xxx series Al MPE tubes without reducing the concentration of Fe. The authors predicted that reducing and dispersing Fe IM particles would impede the corrosion penetration of Al MPE tube. For this purpose, a small amount of zirconium (Zr) alloying which forms Al_3Zr is used to refine the grain and improve the mechanical properties [17–20]. During the homogenization process, the Al_3Zr particle can inhibit grain growth and promote nucleation of other precipitated particles. Therefore, the size of the IM particle around Al_3Zr becomes finer and the dispersion becomes higher. It is expected that adding Zr can aid the refinement and dispersion of corrosive IM particles, thus preventing localized corrosion propagation of the Al MPE tube. Thus, the objective of this study was to investigate the influence of Zr on the refinement and dispersion of IM particles as well as the corrosion propagation property of the Al MPE tube.

2. Experimental methods

2.1. Specimen preparation

In order to evaluate the dispersion effect and corrosion penetration characteristics of the IM particles by Zr, a new alloy (UniCorAl® 1070, U1070) tube was prepared. The U1070 tube has the same concentration of Fe, Si, and Cu as the A1070 commercial Al tube. The A1070 tube (Al-0.10 Fe-0.15 Si without Cu) was provided by Daihan Climate Control Co. (Korea). The composition of the U1070 tube was 0.10 wt% Fe, 0.15 wt% Si, 0.15 wt% Zr, and the remainder was Al. The U1070 tube prepared through the following process: First, 99.9% purity Al ingot (Koralco Co., Korea) and three mother alloys (Fukuoka Al Co., Japan) of Al-20 wt% Fe mother alloy, Al-40% Si mother alloy, and Al-5 wt% Zr mother alloy were charged into a graphite crucible at 710 °C. After all of the components were melted, the degassing process was carried out by the purging of N_2 gas. Mechanical agitation was then performed to uniformly mix all of the alloying elements. The molten metals were injected into a cylinder mold (8-inch in diameter) and air-cooled. Next, they were subjected to homogenization treatment. Extrusion of U1070 was carried out under the same condition as that of A1070. The MPE tube was 1.6 cm wide and 1 mm tall with a wall thickness of 280 μm. The chemical compositions of the MPE tubes were analyzed using ICP-MS, and the results are shown in Table 1.

2.2. Corrosion test

In order to evaluate the corrosion resistance of Al tubes at 49 °C, immersion testing was conducted in a salt-water acetic acid test (SWAAT) solution according to ASTM G85. The penetration depth, shape, and leakage time of the tubes were analyzed. SWAAT solution is the mixed solution of acetic acid and 4.2 wt% NaCl, which has the pH 2.5–3.0. In order to evaluate the corrosion propagation trend and the depth of corrosion, cross-sections were observed by salt-water acetic acid testing (SWAAT) after 7, 14, and 21 days of immersion.

2.3. Analyses of IM particles

Field emission scanning electron microscopy (FE-SEM) and energy dispersion spectroscopy (EDS) with a JSM-7600F (JEOL) SEM were used to analyze the size, shape, and composition of the IM particles. In order to analyze the distribution of the IM particles on cross-sections of the tube specimens, mapping was performed using a field emission electron probe micro analyzer (FE-EPMA) in a JXA-8530F (JEOL). The surfaces of the FE-SEM and FE-EPMA specimens were polished with a 0.05 μm alumina. To remove the oxide layer on the surface, the specimens were

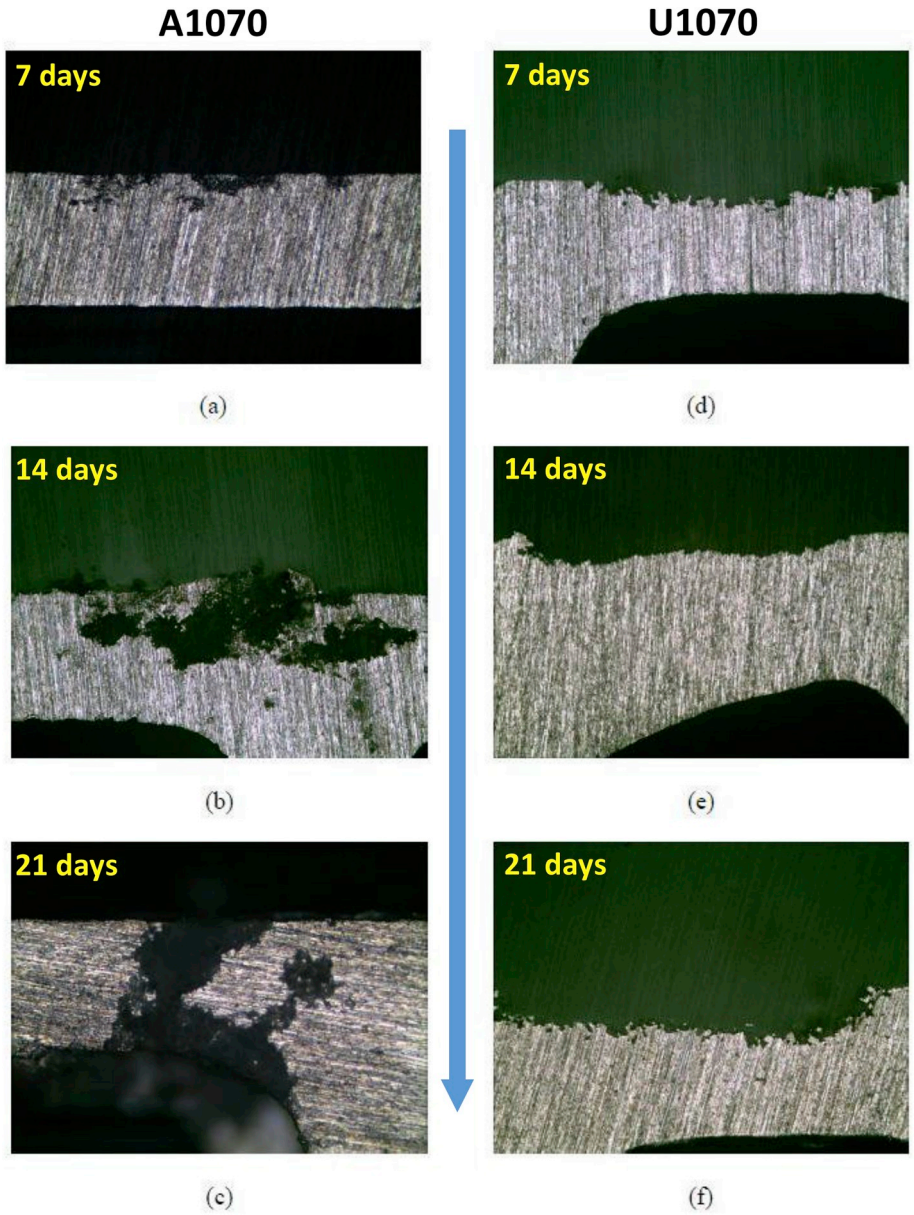

Fig. 1. Cross-sectional images of aluminum tubes after immersion test. (a) 7 days of immersion for A1070, (b) 14 days of immersion for A1070, (c) 21 days of immersion for A1070, (d) 7 days of immersion for U1070, (e) 14 days of immersion for U1070, and (f) 21 days of immersion for U1070.

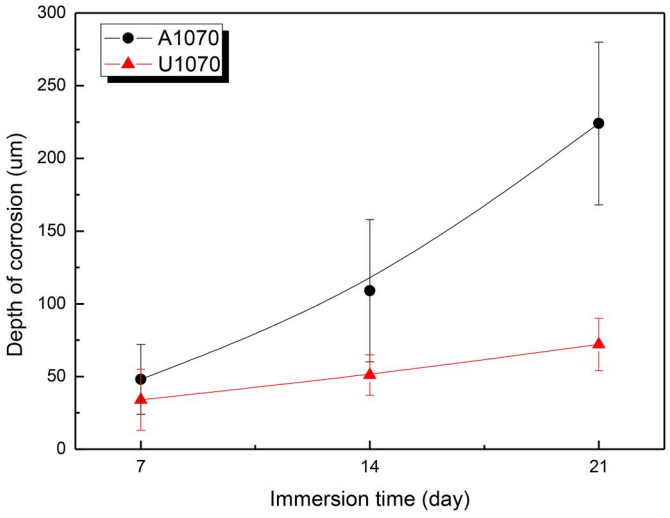

Fig. 2. Change in corrosion depth of aluminum tubes according to immersion time in SWAAT solution.

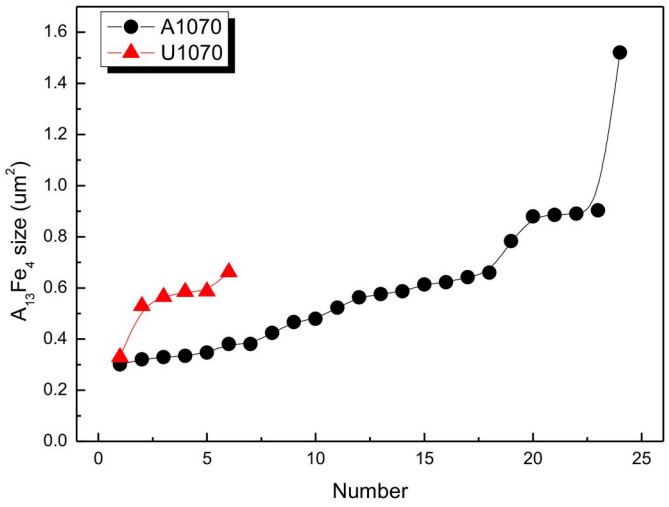

Fig. 4. Size and number of $Al_{13}Fe_4$ particles from FE-SEM images (magnitude: 3,000X) by Image J analysis.

etched in 10% HF solution at room temperature for 30 s, rinsed with distilled water and ethanol, then finally dried with nitrogen gas. In order to observe the IM particles of nanoscale size, high resolution transmitted electron microscopy (HR-TEM) was conducted using a JEM-2100F TEM (JEOL). The thin foils for TEM analysis were prepared by jet polishing at 12 V in a 25% nitric acid and 75% methanol solution cooled to −10 °C in a Tenupol-3 (Struers).

3. Results and discussion

3.1. Corrosion test

Fig. 1 shows the cross-sections of A1070 and U1070 according to the time of immersion testing. The cross-section results show no significant difference between A1070 and U1070. The corrosion at the surface rapidly developed into the inside, and the tube of A1070 was penetrated after 21 days. On the other hand, U1070 showed a uniform corrosion profile. As shown in Fig. 2, the penetration depth of A1070 increased sharply, then finally penetrated. However, U1070 had a remarkably low penetration depth. The results of the immersion experiments confirmed that the leakage of the Al MPE tube was determined by the corrosion propagation behavior while the addition of Zr reduced the corrosion penetration depth of the Al MPE tube.

3.2. Intermetallic particles characterization

The microstructures of A1070 and U1070 are very similar, which

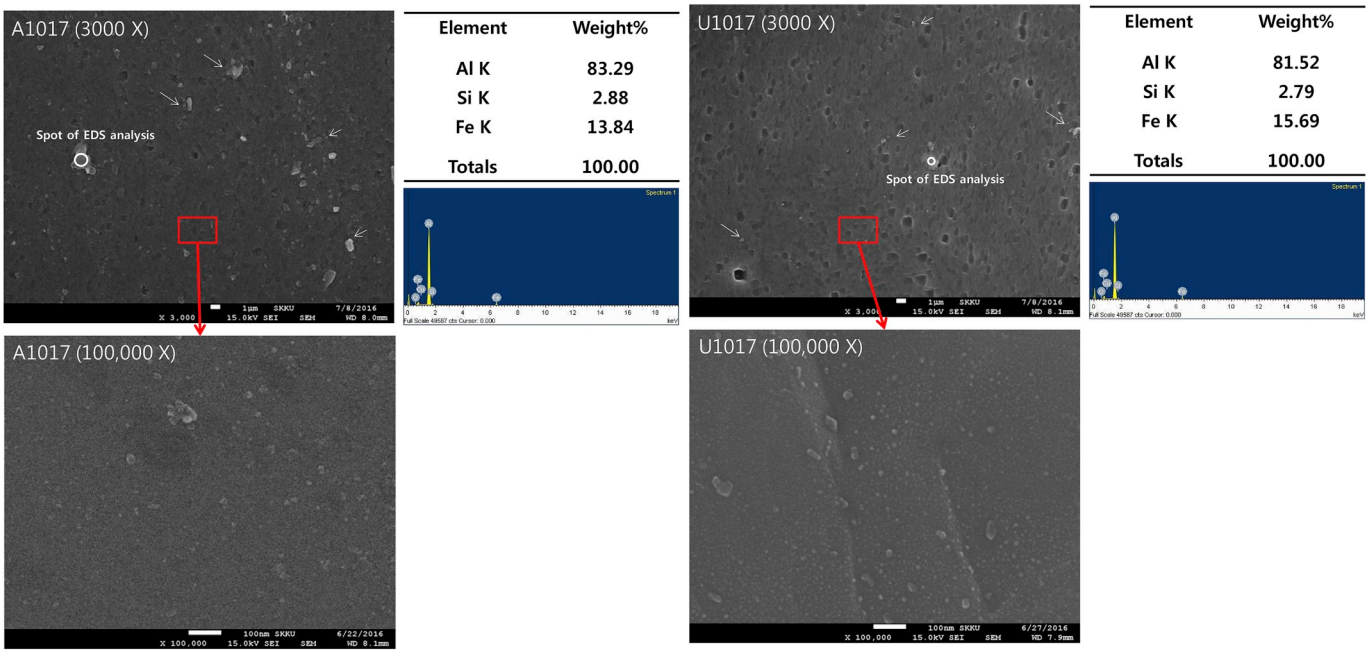

Fig. 3. FE-SEM images (magnitude: 3,000X and 100,000X) and EDS analysis of IM particle (white point: spot of EDS analysis, white arrows: Al–Fe IMs). (a) A1070, (b) U1070.

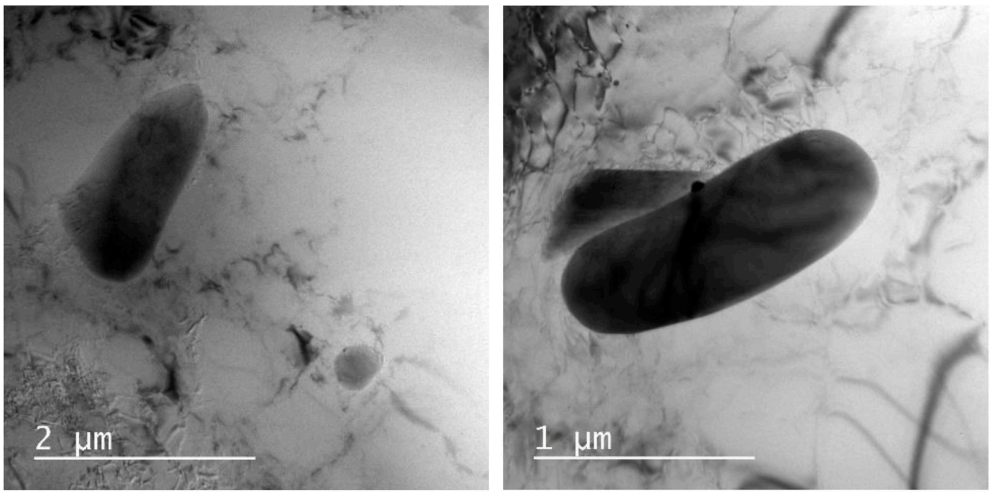

Fig. 5. HR-TEM images of IM particle in A1070.

means that the difference of corrosion property can not depend on the microstructure. Thus, this study focused on analyzing difference of intermetallic particles in both Al alloys.

3.2.1. Results of FE-SEM and EDS

Fig. 3 shows the results of FE-SEM and EDS analyses of A1070 and U1070 tubes. At 3000 × magnification, numerous bright particles were observed on A1070, whereas only a few particles were observed on U1070. EDS analysis was performed on the precipitate phase by bright contrast. The EDS results revealed that these particles were Al–Fe with small amounts of Si. Although Si was found in the EDS results, it would be an insignificant foreign substance in the IM particle. Thus, this IM particle can be considered to be an Al–Fe IM particle. The numbers and sizes of Al–Fe particles were analyzed using Image-J software, and the results are shown in Fig. 4. The area of the bright site of the FE-SEM was measured at an image with 3000 × magnification, and the number of particles larger than 0.3 μm^2 in area was calculated. As shown in Fig. 4, A1070 had 24 particles, and the largest particle had an area of more than 1.8 μm^2. On the other hand, only six particles with an area larger than 0.3 μm^2 were observed on U1070. The average particle size of U1070 (0.54 μm^2) was slightly smaller than that of A1070 (0.60 μm^2). The Fe content of U1070 was similar to that of A1070. However, the sizes and amounts of Al–Fe precipitates on U1070 were decreased at 3000 × magnification. At a higher magnification, more nano-size particles could be observed on U1070 compared to those on A1070. The smaller particles observed on U1070 could be Al–Zr and Al–Fe particles, although they were not analyzed due to the resolution limits of EDS analysis. In previous study [21], it suggested that the size and the number of intermetallic compound in Al matrix influenced the corrosion property. Thus, the increase of the size and the number of particles should be related to the corrosion properties of Al alloy. Finally, TEM analysis was performed to determine the characteristics of nano-size particles on A1070 and U1070.

3.2.2. Results of TEM

Fig. 5 shows HR-TEM images of IM particles on A1070. As mentioned in the previous section describing FE-SEM and EDS, they could be Al–Fe particles. The shape of the IM particle was elliptical, with an average diameter of roughly 1 μm. On the other hand, Al–Zr and Al–Fe IM particles were observed on U1070 (Fig. 6). The shape and diameter of the IM particles were circular and almost 10 nm, respectively. The size of the IM particle on U1070 was much smaller than that on A1070, suggesting that the growth of IM particle was suppressed by the addition of Zr in U1070.

The results of phase analysis of the selected area diffraction pattern (SADP) of each particle in U1070 are shown in Fig. 7. The results clearly confirmed that the IM particles in U1070 were Al_3Zr and $Al_{13}Fe_4$. Further, in the case of $Al_{13}Fe_4$, it indicates that unabsorbed Si phase was a cubic structure of $Al_{13}Fe_4$. Because the electrochemical potentials of Si-absorbed $Al_{13}Fe_4$ and $Al_{13}Fe_4$ are similar to each other [22–25], both particles are expected to have the same influence on the corrosion property of Al. The diameter of the Al_3Zr particle ranged from about 20 to 50 nm, similar to the results of previous studies [26–28]). The diameter of the $Al_{13}Fe_4$ particle in U1070 was measured to be about 80–520 nm. This was much smaller than that of $Al_{13}Fe_4$ particle in A1070, which had a diameter of 1–2.5 μm. This size difference would be related to the difference of average particle size in the results of the SEM analysis.

3.2.3. Results of FE-EPMA

FE-EPMA analysis was conducted to evaluate the $Al_{13}Fe_4$ distribution of the two tubes. The results are shown in Fig. 8. FE-EPMA analysis mapped 20 μm × 20 μm sections. $Al_{13}Fe_4$ particles were clearly observed with a diameter over 1 μm. The difference in $Al_{13}Fe_4$ dispersion between A1070 and U1070 was remarkable. In the case of A1070, about 25 $Al_{13}Fe_4$ particles were distributed at intervals of a few um. In the case of U1070, only one or two $Al_{13}Fe_4$ particles were observed in the analysis area. Schematic models explaining the relationship between the existence of IMs and the corrosion propagation behaviors of Al tubes are shown in Fig. 9. Based on the Al–Fe phase diagram [12], some portion of Fe may precipitate (primary IM particle) while Al billet is air-cooled after casting, and the remaining Fe may exist in an unstable supersaturated state. During homogenization treatment to stabilize the structure and precipitation phase, supersaturated Fe precipitated as a stable $Al_{13}Fe_4$ phase (Secondary IM particle). In the case of A1070, primary and secondary $Al_{13}Fe_4$ grew to a diameter over 1 μm, and the interval distance between IM particles was relatively short. Therefore, corroded zones around the $Al_{13}Fe_4$ of A1070 could have overlapped with each other in a 'net-structure'. This indicates that the continuous distribution of $Al_{13}Fe_4$ is responsible for the continuous propagation of corrosion in the A1070 tube. Regarding U1070, Al_3Zr precipitated during the homogenization process, which refined and dispersed secondary $Al_{13}Fe_4$. Consequently, the amount of $Al_{13}Fe_4$ with a diameter over 1 μm was reduced, and the interval distance between IM particles was very long. In other words, the corroded zones around the $Al_{13}Fe_4$ of U1070 are independent as an 'island-structure', and the corrosion behavior

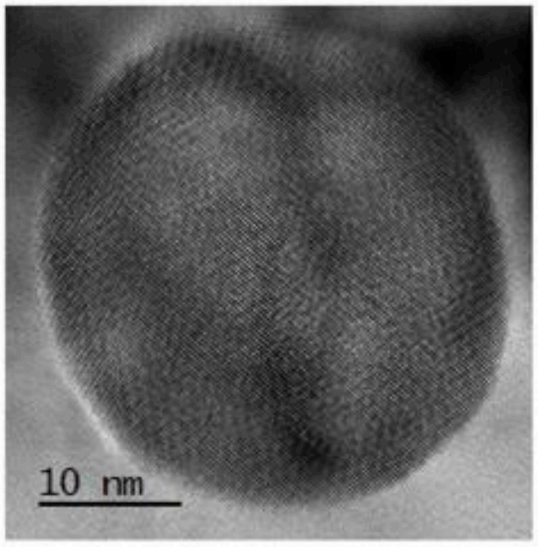

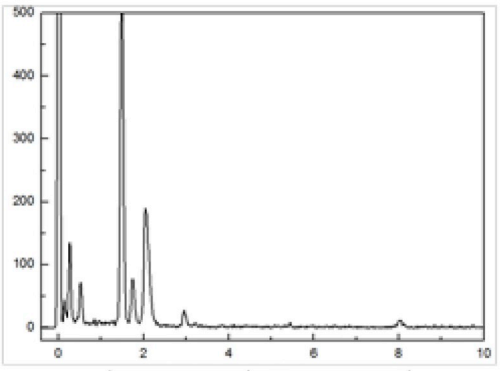

Element	Atomic %
Al	74.04
Zr	26.96

(a)

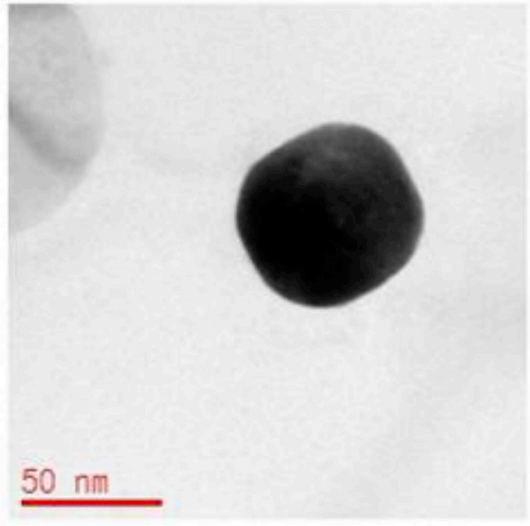

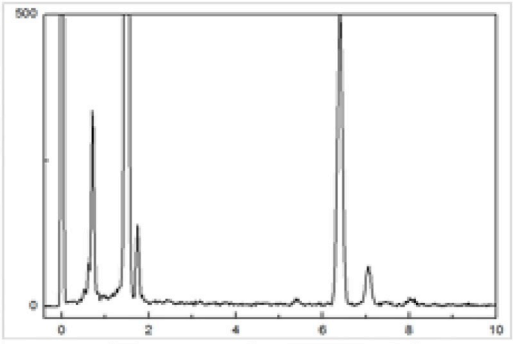

Element	Atomic %
Al	82.5
Si	3.1
Fe	14.4

(b)

Fig. 6. Chemical analysis of IM particles in U1070 tube based on HR-TEM images. (a) Al–Zr particles, (b) Al–Fe particles.

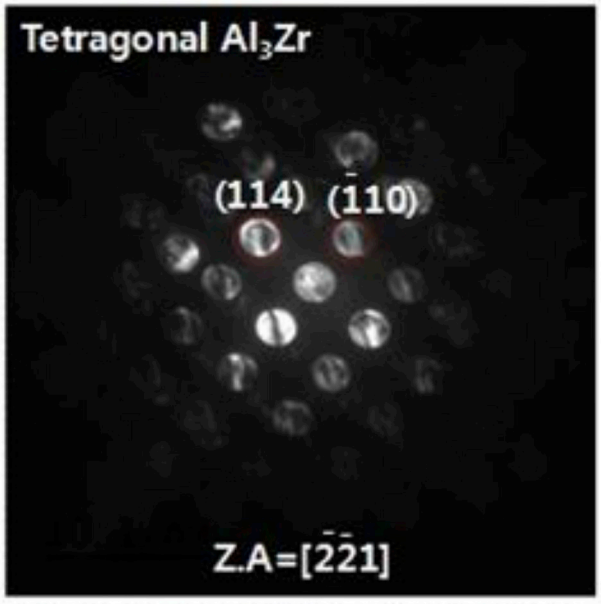

(a)

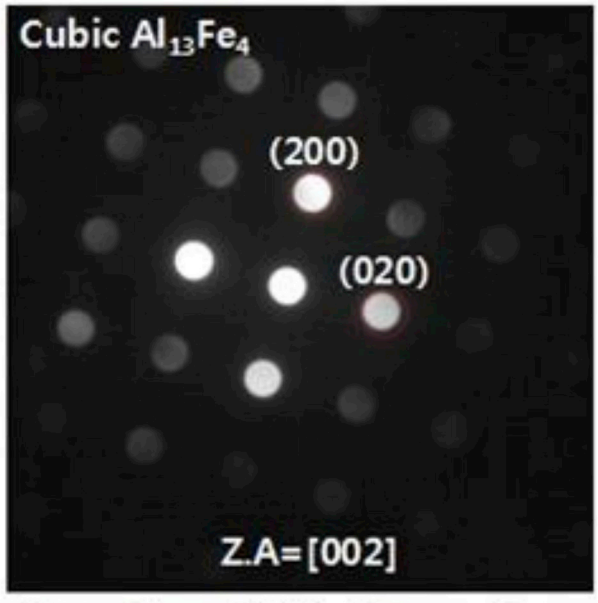

(b)

Fig. 7. Diffraction patterns of IM particles in U1070 tube. (a) Al_3Zr, (b) $Al_{13}Fe_4$.

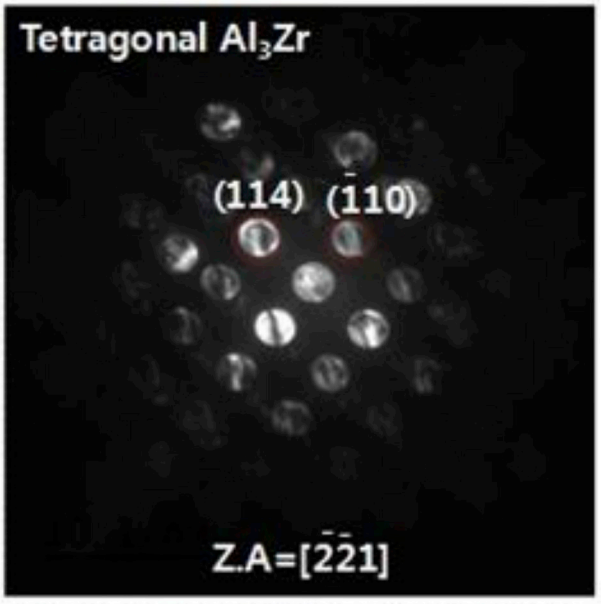

(a)

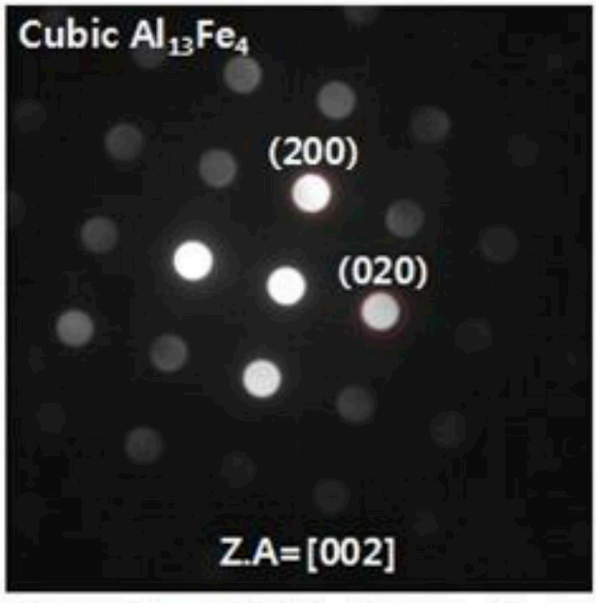

(b)

Fig. 8. Analysis of Al–Fe IM particle distribution by FE-EPMA mapping. (a) A1070, (b) U1070.

becomes relatively discontinuous, thereby suppressing penetration of the tube.

4. Conclusion

In this study, the influence of the addition of Zr on the size and dispersion of IM particles in Al alloys (A1070 and U1070) and the corrosion propagation of the Al tube were investigated. In the immersion corrosion test, the corrosion propagation was found to be much lower in the case of U1070. In addition, the corrosion types between A1070 and U1070 differ from each other. U1070 has a uniform corrosion as opposed to a localized corrosion. The results of IM particle analysis (FE-SEM, FE-TEM, and FE-EPMA) revealed that the addition of Zr made the $Al_{13}Fe_4$ particles finer and dispersed. The refinement and dispersion of $Al_{13}Fe_4$ particles improved the leakage life of the Al tube by changing the corrosion type from localized corrosion to uniform corrosion.

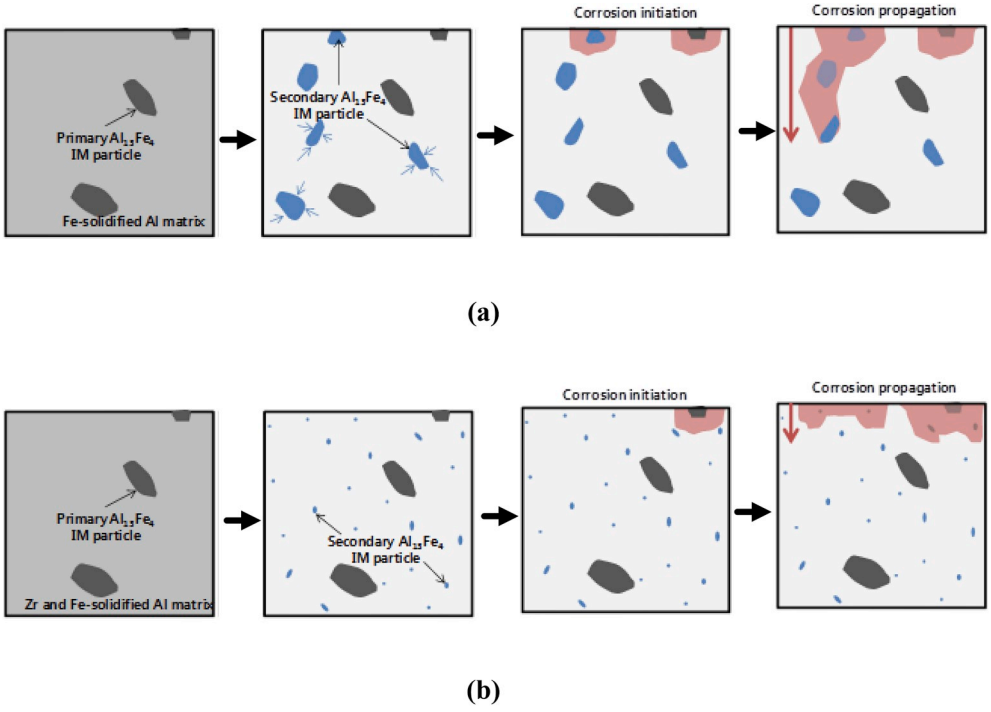

Fig. 9. Schematic model showing the corrosion mechanism of (a) A1070; precipitation of primary $Al_{13}Fe_4$ IM particles after casting → precipitation and growth of secondary $Al_{13}Fe_4$ IM particles during homogenization and extrusion → corrosion initiation around $Al_{13}Fe_4$ IM particles → continuous corrosion propagation through placement of $Al_{13}Fe_4$IM particles (continuous penetration of corrosion), and (b) U1070 tubes; precipitation of primary Al–Fe_4 IM particles after casting → precipitation of refined secondary $Al_{13}Fe_4$ IM particles by Al_3Zr effect during homogenization and extrusion → corrosion initiation around $Al_{13}Fe_4$ IM particles → discontinuous corrosion propagation due to refinement and dispersion of $Al_{13}Fe_4$ IM particles (dispersion of corrosion attack).

References

[1] T.M. Adams, M.F. Dowling, S.I. Abdel-Khalik, S.M. Jeter, Applicability of traditional turbulent single-phase forced convection correlations to non-circular microchannels, Int. J. Heat Mass Transf. 42 (1999) 4411–4415.

[2] W.W. Akers, H.A. Deans, O.K. Crosser, Consideration heat transfer within horizontal tubes, Chem. Eng. Prog. Symp. Ser. 55 (1959) 171–176.

[3] J. Lacaze, S. Tierce, M.C. Lafont, Y. Thebault, N. Pébère, G. Mankowski, C. Blanc, H. Robidou, D. Vaumousse, D. Daloz, Study of the microstructure resulting from brazed aluminum materials used in heat exchanger, Mater. Sci. Eng. A 15 (2005) 413–414.

[4] A. Cavallini, D. Del Col, L. Doretti, M. Matkovic, L. Rossetto, C. Zilio, Condensation heat transfer and pressure gradient inside multiport minichannels, Heat Transf. Eng. 26 (2005) 45–55.

[5] G.J. Marshall, R.K. Bolingbroke, A. Gray, Microstructural control in an aluminium core alloy for brazing sheet applications, Matall. Mater. Trans A 24 (1993) 1935–1942.

[6] M. Shao, Y. Fu, R. Hu, C. Lin, A study on pitting corrosion of aluminium alloy 2024-T3 by scanning microreference electrode technique, Mater. Sci. Eng. A 344 (2003) 323–327.

[7] C. Luo, S.P. Albu, X. Zhou, Z. Sun, X. Zhang, Z. Tang, G.E. Thompson, Continuous and discontinuous localized corrosion of a 2 xxx aluminium-copper-lithium alloy in sodium chloride solution, J. Alloy. Comp. 658 (2016) 61–70.

[8] R. Ambat, A.J. Davenport, G.M. Scamans, A. Afseth, Effect of iron-containing intermetallic particles on the corrosion behaviour of aluminum, Corros. Sci. 48 (2006) 3455–3471.

[9] M.-S. Hong, I.-J. Park, J.-G. Kim, Alloying effect of copper concentration on the localized corrosion of aluminium alloy for heat exchanger tube, Met. Mater. Int. 23 (2017) 708–714.

[10] D.A. Jones, Principles and Prevention of Corrosion, second ed., Prentice-Hall, New Jersey, 1996.

[11] E. Godlewska, Effect of molybdenum on high-temperature corrosion of Fe-Al intermetallics, Intermetallics 14 (2006) 280–286.

[12] X. Li, A. Scherf, M. Heilmajer, F. Stein, The Al-rich part of the Fe-Al phase diagram, J. Phase Equilibria Diffusion 37 (2016) 162–173.

[13] N. Birbilis, R.G. Buchheit, Electrochemical characteristics of intermetallic phases in aluminium alloys, J. Electrochem. Soc. 152 (2005) B140–B151.

[14] R.M. Rynders, C.H. Paik, R. Ke, R.C. Alkire, Use of in situ atomic-force microscopy to image corrosion at inclusions, J. Electrochem. Soc. 141 (1994) 1439–1445.

[15] K. Nisancioğlu, Electrochemical behavior of aluminum-base intermetallics containing iron, J. Electrochem. Soc. 137 (1990) 69–77.

[16] P. Skjerpe, Intermetallic phases formed during DC-casting of an Al–0.25 wt.%, Fe—0.13 wt.% Si alloy, Metall. Trans. A. 18 (1987) 189–200.

[17] D. Tsivoulas, J.D. Robson, Heterogeneous Zr solute segregation and Al_3Zr dispersoid distributions in Al-Cu-Li alloys, Acta Mater. 93 (2015) 73–86.

[18] D. Tsivoulas, J.D. Robson, C. Sigli, P.B. Prangnell, Interactions between zirconium and manganese dispersoid-forming elements on their combined addition in Al-Cu-Li alloys, Acta Mater. 60 (2012) 5245–5259.

[19] Z. Jia, G. Hu, B. Forbord, J.K. Solberg, Effect of homogenization and alloying elements on recrystallization resistance of Al-Zr-Mn alloys, Mater. Sci. Eng. A 444 (2007) 284–290.

[20] K.E. Knipling, R.A. Karnesky, C.P. Lee, D.C. Dunand, D.N. Seidman, Precipitation evolution in Al-0.1Sc, Al-0.1Zr and Al-0.1Sc-0.1Zr (at.%) alloys during isochronal aging, Acta Mater. 58 (2010) 5184–5195.

[21] Y.-S. Kim, J.G. Park, B.-S. An, Y.H. Lee, C.-W. Yang, J.-G. Kim, Investigation of zirconium effect on the corrosion resistance of aluminum alloy using electrochemical methods and numerical simulation in an acidified synthetic sea salt solution, Materials 11 (2018) 1982.

[22] J. Lapin, L. Ondrus, M. Nazmy, Directional solidification of intermetallic Ti-46Al-2W-0.5Si alloy in alumina moulds, Intermetallics 10 (2002) 1019–1031.

[23] C.T. Rios, S. Milenkovic, R. Caram, Directional growth of Al-Nb-X alloys, J. Cryst. Growth 211 (2000) 466–470.

[24] Y. Han, C. Ban, H. Zhang, H. Nagaumi, Q. Ba, J. Cui, Investigations on the solidification behavior of Al-Fe-Si alloy in an alternating magnetic field, Mater. Trans. 47 (2006) 2092–2098.

[25] A.I. Mardare, A.P. Yadav, A.D. Wieck, M. Stratmann, A.W. Hassel, Combination electrochemistry on Al-Fe alloys, Sci. Technol. Adv. Mater. 9 (2008) 035009–035017.

[26] Z. Jia, G. Hu, B. Forbord, J.K. Solberg, Enhancement of recrystallization resistance of Al-Zr-Mn by two-step precipitation annealing, Mater. Sci. Eng. A 483 (2008) 195–198.

[27] J.D. Robson, Optimizing the homogenization of zirconium containing commercial aluminium alloys using a novel process model, Mater. Sci. Eng. A 338 (2002) 219–229.

[28] J.D. Robson, P.B. Prangnell, Modelling Al_3Zr dispersoid precipitation in multicomponent aluminium alloys, Mater. Sci. Eng. A 352 (2003) 240–250.